Catalysis Science & Technology

PAPER

View Article Online
View Journal | View Issue

Cite this: *Catal. Sci. Technol.*, 2016, **6**, 5684

CuO/cryptomelane catalyst for preferential oxidation of CO in the presence of H_2: deactivation and regeneration†

A. Davó-Quiñonero, M. Navlani-García, D. Lozano-Castelló and A. Bueno-López*

Received 12th February 2016,
Accepted 9th April 2016

DOI: 10.1039/c6cy00329j

www.rsc.org/catalysis

Cryptomelane and CuO/cryptomelane catalysts have been tested in the preferential oxidation of CO in the presence of H_2 (CO-PROX reaction), paying special attention to deactivation and regeneration issues. Cryptomelane was stable during the CO-PROX reactions in ramp experiments until 200 °C and in a long-term isothermal experiment (10 h). Changes neither in the H_2 reducibility and porosity nor in the crystalline phases detected by XRD were observed. On the contrary, CuO/cryptomelane was partially deactivated during the consecutive CO-PROX reaction cycles performed until 200 °C, and the catalytic activity was partially restored by reoxidising the catalyst at 200 °C or 400 °C, the latter temperature being more effective. In spite of the CuO/cryptomelane partial deactivation, the CO-PROX activity of this catalyst was higher than that of cryptomelane once a stable behaviour was achieved. The partial deactivation of CuO/cryptomelane was attributed to the segregation of crystalline phases (hausmannite (Mn_3O_4) and/or hopcalite ($CuMn_2O_4$)), with the segregation of potassium to the surface and decrease in the copper cations' reducibility. The potential contribution to deactivation of the changes in the porous texture of CuO/cryptomelane was ruled out.

1. Introduction

Fuel cells have the potential to replace gradually the internal combustion engines in vehicles and provide power in stationary and portable applications, especially Proton Exchange Membrane Fuel Cells (PEMFC).[1–6] For the appropriate development of these devices, the production of clean H_2 is necessary, and nowadays hydrocarbon reforming is the principal pathway.[7–9] The main drawback of this synthesis route is that the typical effluents coming from hydrocarbon reforming contain about a 10 vol% of CO, which apart from being toxic for people, is a poisoning agent for the platinum-based anode catalysts in PEMFC.[10] Then, it is mandatory to reduce the CO concentration to a trace level below 10 ppm, which is the tolerance level of the Pt catalysts.[2,9,11–13]

For CO removal from reformate gases, the gas stream is treated in a Water Gas Shift (WGS) reactor where most CO is oxidised to CO_2. The concentration of CO in the output stream is about 0.5–1 vol%, but this level is not low enough for the PEMFC requirements. Further purification must be performed, and the preferential oxidation of CO (CO-PROX) is a promising technology.[14,15] The aim of the CO-PROX reaction is to oxidize CO selectively by feeding near stoichiometric O_2 while minimising the H_2 consumption, despite its large excess on stream, and utilization of a selective catalyst is mandatory. An ideal CO-PROX catalyst must be active and selective towards CO oxidation in a range of temperatures between that at the exit of the WGS reactor (200 °C) and that at the entrance of the PEM fuel cell (about 80 °C).[9] Besides, it must have a long-term stability.

A wide variety of CO-PROX catalysts have been proposed, the most extensively studied being those based on noble metals[16,17] (Pt,[18–20] Pd,[21–23] Ru,[24,25] Rh[26] and Au[27–31]), transition metals[32] and multi-metallic systems.[33–35] It is worthy to highlight those based on the copper oxide–ceria system, since these materials constitute one of the most thoroughly studied and promising alternatives to noble metal catalysts.[36–42] The outstanding performance of the CuO/CeO_2 catalysts in CO-PROX is related to the strong interaction between CuO and CeO_2 and to the oxygen storing/releasing capacity of ceria, which leads to the high mobility of the lattice oxygen.[39–41] Other oxides with oxygen storing/releasing capacity (such as Fe_2O_3 (ref. 29) and MnO_2 (ref. 43–46)) have been also studied. Manganese oxides are a very promising option to replace ceria due to their abundance, high oxygen mobility and oxygen storage capacity, apart from their low cost, environmental compatibility and non-toxicity.[47,48] Among manganese oxides, cryptomelane has presented an exceptional catalytic

MCMA group. Inorganic Chemistry Department, Inorganic Chemistry Department, University of Alicante, Carretera de San Vicente s/n. E03080, Alicante, Spain. E-mail: agus@ua.es; Fax: +34 965903454; Tel: +34 965903538

† Electronic supplementary information (ESI) available: Catalytic tests and TEM characterisation. See DOI: 10.1039/c6cy00329j

activity in a wide range of reactions.[49–57] This mineral oxide is based on a well-defined 2 × 2 tunnel structure (tunnel size of 0.46 nm × 0.46 nm) consisting of double chains of edge-shared MnO_6 octahedra and corner-sharing of the double chains,[49,58,59] which gives rise to its general name "Octahedral Molecular Sieve" (OMS). Typically, the average manganese oxidation state in cryptomelane is around 3.8, which is a consequence of the coexistence of Mn^{4+} cations with small amounts of Mn^{3+} and Mn^{2+},[60] and the charge imbalance generated by partial reduction of Mn^{4+} is compensated by interstitial cations, such as K^+.

It is well reported that the catalytic activity of cryptomelane for CO oxidation in the CO-PROX system is improved when finely dispersed CuO species were present,[36,50] which could be related to the strong interaction between the highly dispersed CuO and the support.[61] On the other hand, it has been also addressed[43,62] that the CO-PROX activity of CuO/cryptomelane decreases significantly upon reduction under reaction conditions and that part of the activity can be recovered by further reoxidation. However, the initial activity of the catalyst is not recovered and little is known about the changes occurring on the catalyst leading to such activity decay.

The goal of the current study is to get further insights into the causes of the CuO/cryptomelane partial deactivation during the CO-PROX reaction, paying attention to the potential segregation of secondary phases and to the changes in the redox properties of the catalyst.

2. Experimental details

2.1. Catalyst preparation

Synthetic cryptomelane was prepared using the previously described reflux method.[51,52,56] 11 g of manganese(II) acetate was dissolved in 40 g of water and the pH of the solution was fixed at 5 using glacial acetic acid. Then, it was heated and maintained at the boiling temperature under reflux for 30 min. After that, a solution of 6.5 g of potassium permanganate dissolved in 150 ml of water was added, and the mixture was kept under reflux by vigorous stirring for 24 h. The solid was filtered, washed with distilled water until neutral pH and dried at 120 °C overnight. Finally, it was calcined at 450 °C for 2 h.

A CuO/cryptomelane catalyst was prepared with 5 wt% of copper by incipient wetness impregnation of cryptomelane with a copper(II) nitrate trihydrate (Panreac) water solution. The impregnated solid was dried at 110 °C overnight and calcined at 400 °C for 5 h using a heating ramp of 5 °C min^{-1}.

2.2. CO-PROX catalytic tests

A U-shaped reactor with a 16 mm inner diameter was used to perform CO-PROX experiments, where 150 mg of cryptomelane or CuO/cryptomelane was placed and a gas mixture with 2% CO, 2% O_2, 30% H_2 and He balance was fed to the reactor. The O_2 excess with regard to CO was $\lambda = 2$ (being $\lambda = 1$ for stoichiometric CO-O_2 conditions). The catalytic tests were performed using a heating rate of 2 °C min^{-1} from 25 to 200 °C and a total gas flow rate of 100 ml min^{-1} that was set by means of Mass Flow Controllers (Bronkhorst). The exhaust gases were analysed by gas chromatography in an Agilent Technologies 6890 N device equipped with a CTR I column operating at 80 °C and a TC detector.

Consecutive catalytic cycles were performed in order to evaluate the stability of the catalysts, and after each catalytic cycle the catalysts were treated at 200 °C or 400 °C for 1 h (heating rate 5 °C min^{-1}) in 20 ml min^{-1} of 10% O_2/He. Afterwards, the reactor was cooled down to room temperature and a new catalytic cycle was conducted.

After four consecutive ramp CO-PROX experiments, a further isothermal CO-PROX experiment was also carried out using the same gas mixture (2% CO, 2% O_2, 30% H_2, and balance He). The temperatures were selected to obtain *ca.* 75% CO conversion at the beginning of the isothermal experiments.

2.3. Catalyst characterisation

The catalysts were characterised before and after the catalytic tests. X-ray photoelectron spectroscopy (XPS) analysis was performed by using a K-Alpha spectrophotometer (ThermoScientific) with a high-resolution monochromator. The binding energy was adjusted using the C 1s transition, appearing at 284.6 eV. Binding energy values measured are accurate to ±0.2 eV.

Experiments of temperature-programmed reduction with H_2 (H_2-TPR) were performed using a Micromeritics Pulse ChemiSorb 2705 device. 20 mg of catalyst was placed in a U-shaped reactor and the temperature was increased from room temperature up to 900 °C with a heating rate of 10 °C min^{-1} in 20 ml min^{-1} of 5% H_2 in Ar. In some cases, the catalysts used in the CO-PROX reactions were pretreated *in-situ* in the H_2-TPR device at 200 or 400 °C for 1 h in a 20 ml min^{-1} flow of 10% O_2/Ar.

X-ray diffractograms were recorded in a Bruker D8-Advance diffractometer using Cu Kα radiation (λ = 1.540598 Å). Diffractograms were recorded at 2θ between 10° and 80°. Textural characterisation was carried out by means of N_2 adsorption at −196 °C in an automatic adsorption system, Autosorb-6 by Quantachrome. Prior to adsorption measurements, the catalysts were degassed at 250 °C for 4 h in order to remove any adsorbed impurities. The surface area was calculated by using the BET equation (S_{BET}), and pore size distributions were calculated using the DFT method.

3. Results and discussion

3.1. Catalytic tests

Fig. 1 shows results obtained with fresh catalysts in the CO-PROX reaction. Cryptomelane accelerates CO oxidation above 75 °C and CuO loading lowers the onset temperature, CuO/cryptomelane showing CO oxidation even at room temperature. This improvement of the cryptomelane performance upon CuO loading was already reported by Hernández

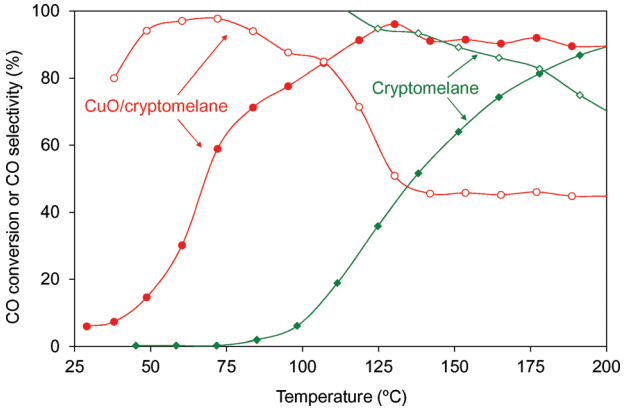

Fig. 1 CO conversion (solid symbols) and CO selectivity (hollow symbols) obtained during the CO-PROX experiments performed with fresh catalysts. Reaction conditions: 150 mg of catalyst, 2% CO, 2% O_2, 30% H_2, balance He, 100 mL min^{-1} 2 °C min^{-1}.

et al.,[63] and was attributed to a high lattice oxygen mobility due to the formation of Cu–O–Mn bridges.

The CO conversion profile of CuO/cryptomelane reached a maximum value near 100% at 130 °C, and then decreased slowly with temperature. This drop in the CO conversion at high temperatures was already reported by other authors and was attributed to the competition between H_2 and CO oxidation and to the formation of hot spots (or higher local temperatures) as a consequence of the exothermic CO and H_2 oxidation reaction, which leads to the reversed WGS reaction and the subsequent CO formation.[18,64]

Thus, the lower activation energy for CO oxidation when comparing to H_2 oxidation favours the preferential process only up to a critical temperature.[37,47]

The selectivity profile of CuO/cryptomelane reached a very high value (~96%) at a relatively low temperature, and then decreased until an almost constant value of about 41%. It is important to highlight that a selectivity of 50% means that equal amounts of CO_2 (desired reaction) and H_2O (side reaction) would be produced and that this is the maximum selectivity achievable at total O_2 consumption in the experimental conditions used (excess oxygen with $\lambda = 2$). Thus, even the relatively low selectivity remaining at high temperatures is high enough to obtain adequate fuel efficiency.[18]

Once confirmed the excellent behaviour of the CuO/cryptomelane catalyst, the stability was studied and four consecutive reaction cycles were performed with the CuO/cryptomelane catalyst under the same experimental conditions used with the fresh catalyst (those indicated in the caption of Fig. 1). For comparison, consecutive reaction cycles were also carried out with cryptomelane. As indicated in the experimental section, after each reaction cycle the catalysts were reoxidised in 10% O_2/He for 1 h. The reoxidation temperature was 200 °C for cryptomelane while two temperatures were tested for CuO/cryptomelane, 200 and 400 °C.

The CO oxidation and CO selectivity curves obtained during these experiments are included in the supplementary material and the T50% temperatures, which is the temperature required to achieve 50% CO oxidation, are plotted in Fig. 2 for the consecutive reaction cycles.

Cryptomelane kept the same activity during the five consecutive reaction cycles, evidencing the high stability of this catalyst. On the contrary, CuO/cryptomelane was partially deactivated during the consecutive cycles, and the temperature of the reoxidation step played an important role. Reoxidation of CuO/cryptomelane at 400 °C was more efficient than reoxidation at 200 °C, and both temperatures allowed stable T50% values to be obtained after the fourth CO-PROX reaction cycle. Despite the CuO/cryptomelane deactivation during the consecutive cycles, the stable T50% values obtained with the copper-containing catalyst in the fourth and fifth cycles were lower than those of cryptomelane, and the lowest values were obtained by reoxidation at 400 °C.

These results in Fig. 2 suggest that the decrease in the CO oxidation capacity of CuO/cryptomelane, once used in the CO-PROX reaction, is related to changes in the copper species, since cryptomelane is stable. This hypothesis was also postulated by other authors[43,62] and will be discussed in more detail in the following sections.

3.2. Long-term catalytic tests

In order to evaluate the stability of the catalysts at constant temperature under CO-PROX reaction conditions, long-term experiments were conducted after the fourth cycle. The temperatures of the isothermal experiments were selected to obtain *ca.* 75% CO conversion.

The CO conversion, CO selectivity and temperature monitored during more than 10 h are shown in Fig. 3a for CuO/cryptomelane and in Fig. 3b for cryptomelane, and both catalysts maintained quite stable behaviours. Only the CuO/cryptomelane catalyst suffered a small drop in CO conversion (~6%) at the beginning of the experiment, which could be related to the presence of copper species because is not observed in copper-free cryptomelane.

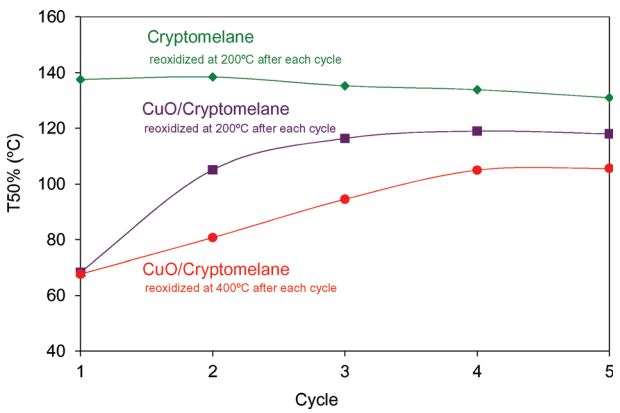

Fig. 2 Temperature for 50% CO oxidation during consecutive CO-PROX reaction cycles. Reaction conditions: 150 mg of catalyst, 2% CO, 2% O_2, 30% H_2, balance He, 100 mL min^{-1} 2 °C min^{-1}. Reoxidation conditions: 1 h in 10% O_2/He, 20 mL min^{-1}, at 200 °C or 400 °C after each CO-PROX cycle.

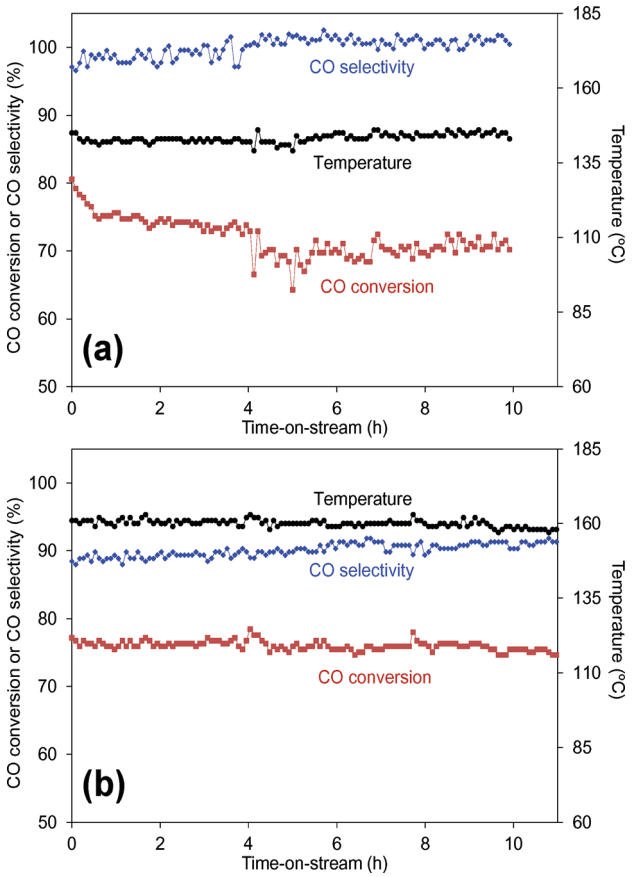

Fig. 3 Long-term CO-PROX experiments performed with (a) CuO/cryptomelane and (b) cryptomelane. Reaction conditions: 150 mg of catalyst, 2% CO, 2% O_2, 30% H_2, balance He, 100 mL min^{-1}.

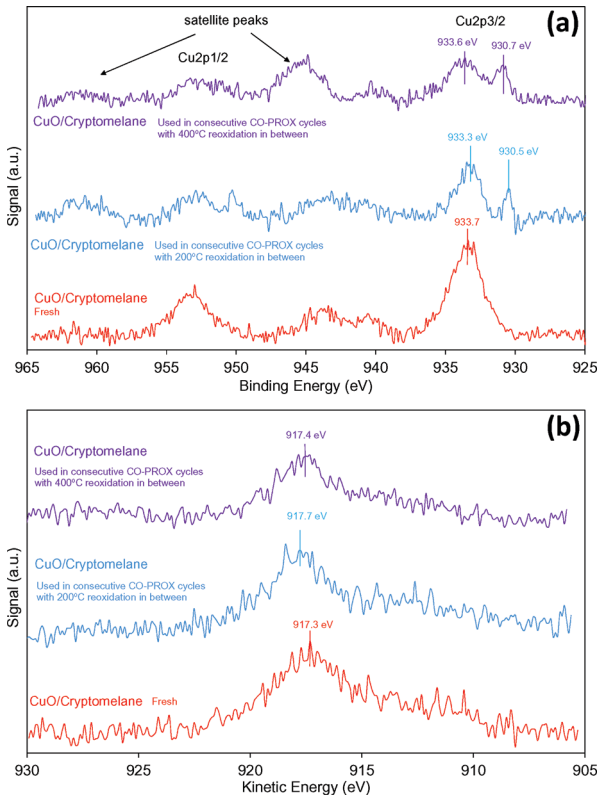

Fig. 4 XPS spectra of CuO/cryptomelane. (a) Cu 2p region and (b) Cu LMM Auger range.

In conclusion, the ramp experiments showed that cryptomelane is stable while CuO/cryptomelane partially deactivates during the consecutive CO-PROX reaction cycles performed from room temperature up to 200 °C. This deactivation was quite small in the long-term experiment performed at 145 °C, indicating that transformations leading to partial deactivation occur above this temperature. The catalytic activity of CuO/cryptomelane was partially restored reoxidising the catalyst, and 400 °C reoxidation was more effective than 200 °C reoxidation.

3.3. XPS characterisation

The ramp CO-PROX experiments suggested that changes in the copper species was the reason for the activity decay of the CuO/cryptomelane catalyst during the consecutive cycles, and XPS was used to analyse these changes during the experiments. Fig. 4 shows the Cu 2p region for fresh CuO/cryptomelane and for this catalyst used after consecutive CO-PROX cycles with reoxidation treatments at 200 °C or 400 °C in between (XPS measurements were done after the fifth CO-PROX cycle). It is worth noting that the used catalyst was not reoxidised after the last CO-PROX cycle.

The Cu $2p_{3/2}$ photoemission of fresh catalyst showed a main contribution at 933.7 eV, typical of CuO,[65] and the used catalyst additionally showed another contribution at 930.5–930.7 eV that must be assigned to copper species with a different negative charge density. These low binding energy values have been reported for Cu–Mn mixed oxide with a hopcalite structure ($CuMn_2O_4$).[66–68] The main cations on hopcalite are Cu(II) and Mn(III), but the presence of Cu(I) has been postulated due to the equilibrium Cu(II) + Mn(III) = Cu(I) + Mn(IV). Evidence of the formation of hopcalite after the catalytic tests has been also obtained in the current study by XRD, as it will be discussed below.

These XPS results suggest that copper was fully oxidised as CuO on the fresh catalyst, which is not surprising because it was calcined for copper precursor decomposition, and part of this CuO was introduced into the hopcalite structure during the ramp CO-PROX experiments while part remained as CuO. The Cu LMM Auger transition (Fig. 4b) is quite similar in all spectra, being consistent with the presence of Cu(II). However, the relative contribution of the Cu(II) satellite peak at 944 eV (Fig. 4a) with regard to the Cu $2p_{3/2}$ peak at ~933.5 eV increases as seen on the spectra obtained with the used catalyst reoxidised at 400 °C with regard to that reoxidised at 200 °C. This suggests a higher population of Cu(II) cations upon 400 °C reoxidation. Nevertheless, identification of the copper species by XPS is complex,[69–72] and much more

concluding evidence was obtained by H_2-TPR, as discussed below.

The surface composition of the cryptomelane and CuO/cryptomelane catalysts was also analysed by XPS, and Table 1 compiles results of the K/Mn and Cu/Mn ratios obtained.

The K/Mn ratio of cryptomelane slightly decreased after the CO-PROX ramp experiments, but this small surface modification does not affect the catalytic performance. On the contrary, the K/Mn atomic ratio of CuO/cryptomelane remained constant after the CO-PROX ramp experiment (without reoxidation) and increased during the consecutive CO-PROX experiments with reoxidation treatments in between, suggesting certain segregation of potassium to the surface. These results indicate that the segregation of K to the surface mainly occurs during the reoxidation treatments when copper is present. This segregation of K to the surface was similarly suggested by Veprek *et al.*[66] for commercial hopcalite tested as a CO oxidation catalyst. Furthermore, Hu *et al.*[73] also described this phenomenon for silver-doped cryptomelane, and in our CuO/cryptomelane catalyst, it occurred to a higher extent when the reoxidation between cycles was performed at 400 °C compared to the reoxidation at 200 °C.

In addition, the Cu/Mn ratio decreased after the CO-PROX reactions performed with reoxidation treatments in between, and the minimum value was obtained for the catalyst reoxidised at 400 °C between cycles. The reduction of this parameter can be an evidence of copper sintering.

These XPS results allowed concluding that the CuO/cryptomelane catalyst suffered segregation of potassium to the surface and copper sintering, which could explain that the initial activity of the fresh catalyst was not fully recovered (see Fig. 2) after the reoxidation treatments. More information about these transformations was obtained by complementary characterisation techniques that are discussed in the coming sections.

3.4. H_2-TPR characterisation

Since the redox processes occurring on CuO/cryptomelane seem to be behind the partial deactivation of this catalyst during the consecutive CO-PROX ramp experiments, H_2-TPR characterization was carried out to get further insight into such processes. Fig. 5 compiles the H_2 reduction profiles obtained with the cryptomelane and CuO/cryptomelane catalysts tested as prepared (fresh) and after CO-PROX experiments (after the fifth CO-PROX cycle).

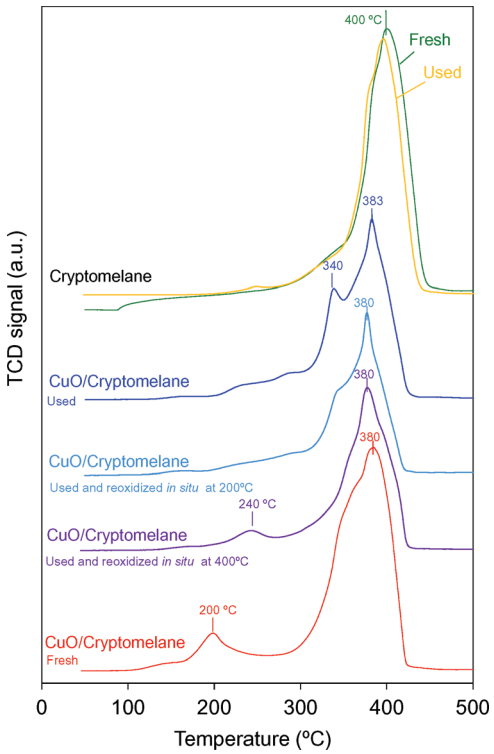

Fig. 5 H_2 reduction profiles obtained with cryptomelane and CuO/cryptomelane catalysts tested as prepared (fresh) and after CO-PROX experiments (after the fifth CO-PROX cycle). In some cases, the used CuO/cryptomelane catalyst was reoxidised *in situ* (in the H_2-TPR device) at 200 or 400 °C (at the same temperature used in each case of the consecutive CO-PROX cycles for reoxidation between cycles).

The H_2-TPR profiles obtained with fresh and used cryptomelane are equal (top profiles in Fig. 5), with a single peak with maxima at 400 °C and a low-temperature shoulder evidencing that several events were taking place. This is consistent with the high stability of this material during the consecutive ramp CO-PROX experiments (Fig. 2). Note that the onset H_2 reduction temperature in H_2-TPR experiments (~270 °C) was well above the maximum temperature achieved in the ramp CO-PROX experiments (200 °C).

The consumption of H_2 by cryptomelane in H_2-TPR experiments is attributed to the reduction of manganese cations, initially present mainly in +4 and +3 oxidation states, giving MnO as the final product of the reduction processes.[74] It is

Table 1 Atomic surface composition of cryptomelane and CuO/cryptomelane determined by XPS

Catalyst	K/Mn	Cu/Mn
Cryptomelane fresh	0.64	—
Cryptomelane (used during the consecutive CO-PROX cycles with 200 °C reoxidation in between)	0.52	—
CuO/cryptomelane fresh	0.58	0.19
CuO/cryptomelane used (without reoxidation)	0.59	0.23
CuO/cryptomelane (used during the consecutive CO-PROX cycles with 200 °C reoxidation in between)	0.65	0.12
CuO/cryptomelane (used during the consecutive CO-PROX cycles with 400 °C reoxidation in between)	0.83	0.06

known that the reduction progresses throughout the following sequence: $MnO_2 \rightarrow Mn_2O_3 \rightarrow Mn_3O_4 \rightarrow MnO$, though it is not easy to discern each step due to the experimental conditions and the local environment of the reducible species.[47,63,75] Hence, cryptomelane has a complex reduction profile with several chemical transformations appearing under the same peak.[76–79] Typically, the H_2 reduction profiles of cryptomelane described in bibliography, which are similar to those on Fig. 5, consist of a shoulder at about 340 °C, assigned to the reduction of surface cations, followed by a main peak attributed to bulk transformations of MnO_2/Mn_2O_3 to Mn_3O_4, and Mn_3O_4 to MnO, which overlap in the H_2-TPR profile.

The H_2 reduction profile of fresh CuO/cryptomelane (bottom curve on Fig. 5) had some differences compared to that of bare cryptomelane (top curve on Fig. 5). A H_2 consumption peak was observed at 200 °C associated to the reduction of disperse CuO particles. It must be taken into account that bulk CuO is reduced above 350 °C,[65] and the shift to lower temperature in CuO/cryptomelane must be attributed to the effect of the cryptomelane support.[45,46] In addition, the reduction of cryptomelane also took place at a lower temperature in CuO/cryptomelane (maximum at 380 °C) than in bare cryptomelane (400 °C). It has been reported that the addition of copper leads to the creation of Cu^{2+}–O–Mn^{y+} entities that promote the oxygen lability with partial delocalization of the Mn–O bond, improving manganese reducibility.[46,62,63,76,77] Such lability is related to a high structural and superficial oxygen mobility, and this is positive for oxidation reactions occurring throughout a Mars van Krevelen mechanism, which is usually accepted for these kinds of catalysts.[49,62,80] In the reaction studied in this article, it is expected that CO was oxidised by the catalytic oxygen, forming oxygen vacancies that were filled up by gas phase molecular oxygen afterwards.[81]

Moreover, it has been reported that metallic Cu has a catalytic effect on the dissociation of the H_2 molecule, and enhances the reduction of interfacial manganese cations by hydrogen spillover.[20,46,77] This effect is strongly dependent on the CuO dispersion.[82,83] The catalytic effect of metallic copper would explain the shift of the main manganese reduction peak from 400 to 380 °C.

The H_2 reduction profile of fresh CuO/cryptomelane changed after the ramp CO-PROX reaction (see reduction profile of used CuO/cryptomelane in Fig. 5). The peak at 200 °C associated to the reduction of highly dispersed CuO species disappeared, indicating that CuO was reduced under the reaction conditions of the CO-PROX ramp experiments. Instead, two little reduction events were identified at 240 and 280 °C, probably due to the reduction of CuO aggregates with two different sizes[62] that remained oxidised after the CO-PROX experiments. Additionally, the main band at 380–400 °C attributed to manganese cation reduction was also different for fresh and used CuO/cryptomelane. The low-temperature shoulder observed in the fresh catalyst became a well-defined peak in the used catalyst. This could indicate that oxygen species were accumulated on the catalyst surface during the CO-PROX reaction, which would be reduced in the H_2-TPR experiments, and the desorption of carbonate/bicarbonate species accumulated on the catalyst as CO oxidation intermediates cannot be ruled out.

The reoxidation of the used CuO/cryptomelane catalyst at 200 °C had a little effect on the H_2 reduction profile. The low temperature CuO reduction peak remained missing, evidencing that this temperature was not high enough to reoxidise copper. The main difference in the H_2 reduction profiles of the used CuO/cryptomelane catalyst before and after reoxidation at 200 °C was the decrease in the peak at 340 °C, which indicates that this reoxidation treatment removed surface species accumulated during the CO-PROX reaction.

Nevertheless, used CuO/cryptomelane reoxidation at 400 °C leads to the oxidation of reduced copper, and a H_2 reduction peak appeared at 240 °C. This temperature was higher than that on the fresh catalyst (200 °C), and the worse reducibility of CuO after reduction and reoxidation could explain the partial decrease in the CO oxidation capacity during the consecutive CO-PROX cycles (see Fig. 2). This worse reduction of CuO after reoxidation at 400 °C could be due to the worse CuO–cryptomelane interaction[68,84,85] and is consistent with the evidence of copper sintering provided by XPS (see Table 1).

3.5. Characterisation by XRD and N_2 adsorption–desorption

The structural transformations of the catalysts during the ramp CO-PROX experiments were studied, and Fig. 6 shows the X-ray powder diffraction (XRD) patterns of fresh and used cryptomelane and CuO/cryptomelane.

All diffractograms showed the main reflections of the cryptomelane structure, while evidence of the CuO peaks were not observed in the diffractograms of CuO/cryptomelane. This indicated that CuO aggregates must consist of small crystallites.[36,86]

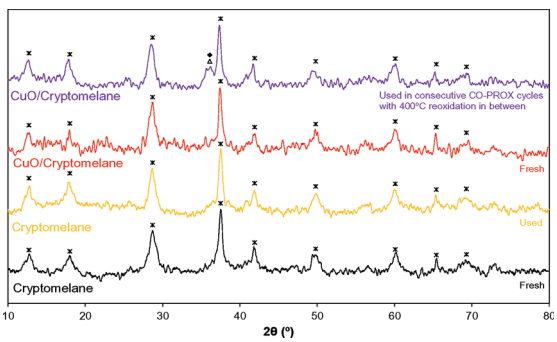

Fig. 6 X-Ray powder diffraction patterns for: (a) fresh cryptomelane; (b) used cryptomelane; (c) fresh CuO/cryptomelane; (d) used CuO/cryptomelane after 5 consecutive CO-PROX cycles with 400 °C reoxidation in between. (*) Cryptomelane (JCPDS card no. 29-1020); (Δ) $CuMn_2O_4$, (JCPDS card no. 45–0505); (♦) Mn_3O_4, hausmannite (JCPDS card no. 24–0734); (□) CuO (JCPDS card no. 80–1268).

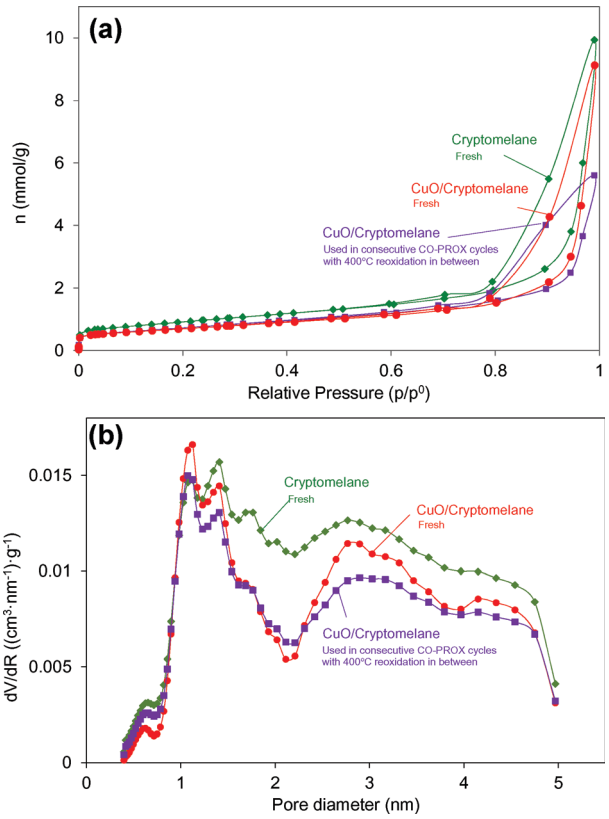

Fig. 7 N_2 adsorption–desorption isotherm (−196 °C) characterization for fresh cryptomelane, fresh CuO/cryptomelane and used CuO/cryptomelane after 5 consecutive CO-PROX cycles with 400 °C reoxidation in between. (a) N_2 adsorption–desorption isotherm and (b) pore size distribution calculated by the DFT method.

The cryptomelane catalyst showed the same diffractogram before and after the ramp CO-PROX experiments, which was in good agreement with the high stability of this material under reaction conditions (see Fig. 2). On the contrary, an additional peak appeared on the diffractogram of CuO/cryptomelane after the CO-PROX experiments that could be attributed to hausmannite (Mn_3O_4) and/or to hopcalite ($CuMn_2O_4$). Cryptomelane, hausmannite and hopcalite are based on tetragonal structures, and seldom transitions can take place as a consequence of partial reduction of manganese cations and/or due to the sintering of copper particles to form copper–manganese mixed oxide aggregates. These transformations are in agreement with the surface restructuration observed by XPS (Table 1) and with the worse reduction of CuO observed in H_2-TPR profiles (Fig. 5), and also explain why the CO oxidation capacity of CuO/cryptomelane was not fully recovered after reoxidation at 400 °C (Fig. 2).

Finally, selected samples were characterised by N_2 adsorption–desorption at −196 °C. Fig. 7a shows the N_2 adsorption–desorption isotherms for fresh cryptomelane, fresh CuO/cryptomelane and CuO/cryptomelane used during the 5 consecutive CO-PROX cycles with 400 °C reoxidation in between, and Fig. 7b shows the pore size distributions calculated by the DFT method. The obtained specific surface areas are compiled in Table 2.

Table 2 Catalyst characterization by gas adsorption–desorption

Catalyst	S_{BET} ($m^2\ g^{-1}$)
Cryptomelane fresh	73
CuO/cryptomelane fresh	59
CuO/cryptomelane used during the consecutive CO-PROX cycles with 400 °C reoxidation in between	55

Cryptomelane showed a type IV N_2 adsorption isotherm, with a hysteresis loop in the high relative pressure range, which according to the IUPAC classification is typical of mesoporous materials. Cryptomelane-based materials show a type H3 hysteresis, as it does not exhibit any limiting adsorption at high P/P_0, and this is typical of non-rigid aggregates of plate-like particles giving rise to slit-shaped pores.[87]

The N_2 adsorption–desorption isotherms of fresh and used CuO/cryptomelane were qualitatively similar to that of cryptomelane, but with a slightly lower adsorption at low relative partial pressures. This decrease could be attributed to the partial porosity blocking by CuO. This is confirmed by the pore size distributions (Fig. 7b). Fresh cryptomelane shows porosity in the 1–5 nm range, as expected, and CuO decreases porosity at around 2 nm. The surface area values are also consistent with the decrease upon CuO loading, being 73 $m^2\ g^{-1}$ for cryptomelane and 59 $m^2\ g^{-1}$ for CuO/cryptomelane, and these values are in agreement with those reported by other authors.[51,62,80,88] Further changes in the porosity of the CuO/cryptomelane catalyst during the ramp CO-PROX reactions were negligible, indicating that the restructuration detected by XPS and XRD does not affect the porosity.

4. Conclusions

In conclusion, the study of cryptomelane and CuO/cryptomelane catalysts in the CO-PROX reaction, paying special attention to deactivation and regeneration, has shown that:

- Cryptomelane was stable during the CO-PROX reactions in ramp experiments until 200 °C and in a long-term isothermal experiment (10 h). Changes neither in the H_2 reducibility and porosity nor in the crystalline phases detected by XRD were observed.
- CuO/cryptomelane was partially deactivated during the consecutive CO-PROX reaction cycles performed until 200 °C, and the catalytic activity was partially restored by reoxidising the catalyst at 200 °C or 400 °C, the latter temperature being more effective.
- In spite of the CuO/cryptomelane partial deactivation, the catalytic CO-PROX activity of this catalyst was higher than that of cryptomelane once a stable behaviour was achieved.
- The partial deactivation of CuO/cryptomelane was related to the segregation of crystalline phases (hausmannite (Mn_3O_4) and/or to hopcalite ($CuMn_2O_4$)), with segregation of

potassium to the surface and decrease in the copper cations' reducibility. The potential contribution to the deactivation of changes in the porous texture of the CuO/cryptomelane catalyst has been ruled out.

Acknowledgements

The authors are thankful for the financial support from Generalitat Valenciana (Project PROMETEOII/2014/010), the Spanish Ministry of Economy and Competitiveness (Project MAT2014-61992-EXP and CTQ2015-67597-C2-2-R), the Spanish Ministry of Education, Culture and Sports (grant FPU14/01178), the Spanish Catalysis Society (SECAT TFM 2015), and the UE (FEDER funding).

Notes and references

1 P. G. Gray and M. I. Petch, *Platinum Met. Rev.*, 2000, **44**, 108.
2 T. V. Choudhary and D. W. Goodman, *Catal. Today*, 2002, **77**, 65.
3 S. Bashir and J. Liu, *Advanced Nanomaterials and Their Applications in Renewable Energy*, Elsevier Inc., 2015, p. 233.
4 C. Fiori, A. Dell'Era, F. Zuccari, A. Santiangeli, A. D'Orazio and F. Orecchini, *Int. J. Hydrogen Energy*, 2015, **40**, 11949.
5 C. Liu and C. Sung, *J. Power Sources*, 2012, **220**, 348.
6 Y. Wang, K. S. Chen, J. Mishler, S. C. Cho and X. C. Adroher, *Appl. Energy*, 2011, **88**, 981.
7 J. N. Armor, *Appl. Catal., A*, 1999, **176**, 159.
8 J. N. Armor, *Prepr. Symp. - Am. Chem. Soc., Div. Fuel Chem.*, 2000, **45**, 165.
9 R. Farrauto, S. Hwang, L. Shore, W. Ruettinger, J. Lampert, T. Giroux, Y. Liu and O. Ilinich, *Annu. Rev. Mater. Res.*, 2003, **33**, 1.
10 T. V. Reshetenko, K. Bethune, M. A. Rubio and R. Rocheleau, *J. Power Sources*, 2014, **269**, 344.
11 N. Bion, F. Epron, M. Moreno, F. Mariño and D. Duprez, *Top. Catal.*, 2008, **51**, 76.
12 A. F. Ghenciu, *Curr. Opin. Solid State Mater. Sci.*, 2002, **6**, 389.
13 E. D. Park, D. Lee and H. C. Lee, *Catal. Today*, 2009, **139**, 280.
14 M. A. Ashraf, G. Ercolino, S. Specchia and V. Specchia, *Int. J. Hydrogen Energy*, 2014, **39**, 18109.
15 G. Ercolino, M. A. Ashraf, V. Specchia and S. Specchia, *Appl. Energy*, 2015, **143**, 138.
16 F. Mariño, C. Descorme and D. Duprez, *Appl. Catal., B*, 2004, **54**, 59.
17 S. H. Oh and R. M. Sinkevitch, *J. Catal.*, 1993, **142**, 254.
18 M. J. Kahlich, H. Gasteiger and R. J. Behm, *J. Catal.*, 1997, **171**, 93.
19 A. Wootsch, C. Descorme and D. Duprez, *J. Catal.*, 2004, **225**, 259.
20 K. Liu, A. Wang and T. Zhang, *ACS Catal.*, 2012, **2**, 1165.
21 I. Miguel-García, Á. Berenguer-Murcia and D. Cazorla-Amorós, *Appl. Catal., B*, 2010, **98**, 161.
22 I. Rosso, C. Galletti, G. Saracco, E. Garrone and V. Specchia, *Appl. Catal., B*, 2004, **48**, 195.
23 M. Navlani-García, I. Miguel-García, A. Berenguer-Murcia, D. Lozano-Castelló, D. Cazorla-Amorós and H. Yamashita, *Catal. Sci. Technol.*, 2015, **5**, 364.
24 Y. Han, M. J. Kahlich, M. Kinne and R. J. Behm, *Phys. Chem. Chem. Phys.*, 2002, **4**, 389.
25 S. Chin, O. Alexeev and M. Amiridis, *Appl. Catal., A*, 2005, **286**, 157.
26 C. Galletti, S. Specchia, G. Saracco and V. Specchia, *Ind. Eng. Chem. Res.*, 2008, **47**, 5304.
27 M. M. Schubert, *J. Catal.*, 2001, **197**, 113.
28 B. Schumacher, Y. Denkwitz, V. Plzak, M. Kinne and R. J. Behm, *J. Catal.*, 2004, **224**, 449.
29 T. Shodiya, O. Schmidt, W. Peng and N. Hotz, *J. Catal.*, 2013, **300**, 63.
30 R. J. H. Grisel and B. E. Nieuwenhuys, *J. Catal.*, 2001, **199**, 48.
31 A. Luengnaruemitchai, S. Osuwan and E. Gulari, *Int. J. Hydrogen Energy*, 2004, **29**, 429.
32 F. Mariño, C. Descorme and D. Duprez, *Appl. Catal., B*, 2005, **58**, 175.
33 S. Y. Chin, O. S. Alexeev and M. D. Amiridis, *J. Catal.*, 2006, **243**, 329.
34 M. M. Schubert, M. J. Kahlich, G. Feldmeyer, M. Hüttner, S. Hackenberg and H. A. Gasteiger, *Phys. Chem. Chem. Phys.*, 2001, **3**, 1123.
35 L. E. Gómez, B. M. Sollier, M. D. Mizrahi, J. M. Ramallo-López, E. E. Miró and A. V. Boix, *Int. J. Hydrogen Energy*, 2014, **39**, 3719.
36 M. Monte, D. Gamarra, A. López-Cámara, S. B. Rasmussen, N. Gyorffy, Z. Schay, A. Martínez-Arias and J. C. Conesa, *Catal. Today*, 2014, **229**, 104.
37 A. Martínez-Arias, D. Gamarra, A. B. Hungría, M. Fernández-García, G. Munuera, A. Hornés, P. Bera, J. C. Conesa and A. López-Cámara, *Catalysts*, 2013, **3**, 378.
38 D. Gamarra, G. Munuera, A. B. Hungría, M. Fernández-García, J. C. Conesa, P. A. Midgley, X. Q. Wang, J. C. Hanson, J. A. Rodríguez and A. Martínez-Arias, *J. Phys. Chem. C*, 2007, **111**, 11026.
39 T. Caputo, L. Lisi, R. Pirone and G. Russo, *Appl. Catal., A*, 2008, **348**, 42.
40 H. Zou, X. Dong and W. Lin, *Appl. Surf. Sci.*, 2006, **253**, 2893.
41 C. S. Polster, H. Nair and C. D. Baertsch, *J. Catal.*, 2009, **266**, 308.
42 A. Hornés, A. B. Hungría, P. Bera, A. López-Cámara, M. Fernández-García, A. Martínez-Arias, L. Barrio, M. Estrella, G. Zhou, J. J. Fonseca, J. C. Hanson and J. A. Rodríguez, *J. Am. Chem. Soc.*, 2010, **132**, 34.
43 Y. I. Hasegawa, R. U. Maki, M. Sano and T. Miyake, *Appl. Catal., A*, 2009, **371**, 67.
44 G. J. Hutchings, A. A. Mirzaei, R. W. Joynerb, M. R. H. Siddiqui and S. H. Taylor, *Appl. Catal., A*, 1998, **166**, 143.
45 E. C. Njagi, H. C. Genuino, C. K. King'ondu, C.-H. Chen, D. Horvath and S. L. Suib, *Int. J. Hydrogen Energy*, 2011, **36**, 6768.
46 K. Qian, Z. Qian, Q. Hua, Z. Jiang and W. Huang, *Appl. Surf. Sci.*, 2013, **273**, 357.

47 K. Ramesh, L. Chen, F. Chen, Y. Liu, Z. Wang and Y. Han, *Catal. Today*, 2008, **131**, 477.
48 R. Craciun, B. Nentwick, K. Hadjiivanov and H. Knözinger, *Appl. Catal., A*, 2003, **243**, 67.
49 C.-H. Chen, S. L. Suib and J. Chinese, *Chem. Soc. Rev.*, 2012, **59**, 465.
50 J. Chen, J. Li, H. Li, X. Huang and W. Shen, *Microporous Mesoporous Mater.*, 2008, **116**, 586.
51 I. Atribak, A. Bueno-López, A. García-García, P. Navarro, D. Frías and M. Montes, *Appl. Catal., B*, 2010, **93**, 267.
52 J. Luo, Q. Zhang, A. Huang and S. L. Suib, *Microporous Mesoporous Mater.*, 2000, **35-36**, 209.
53 V. P. Santos, M. F. R. Pereira, J. J. M. Órfão and J. L. Figueiredo, *Top. Catal.*, 2009, **52**, 470.
54 P. H. Ho, S. C. Lee, J. Kim, D. Lee and H. C. Woo, *Fuel Process. Technol.*, 2015, **131**, 238.
55 H. Tian, J. He, X. Zhang, L. Zhou and D. Wang, *Microporous Mesoporous Mater.*, 2011, **138**, 118.
56 Y. F. Shen, R. P. Zerger, R. N. DeGuzman, S. L. Suib, L. McCurdy, D. I. Potter and C. L. O'Young, *Science*, 1993, **260**, 511.
57 H. C. Genuino, S. Dharmarathna, E. C. Njagi, M. C. Mei and S. L. Suib, *J. Phys. Chem. C*, 2012, **116**, 12066.
58 S. L. Suib, *Curr. Opin. Solid State Mater. Sci.*, 1998, **3**, 63.
59 H. C. Genuino, Y. Meng, D. T. Horvath, C.-H. Kuo, M. S. Seraji, A. M. Morey, R. L. Morey, R. L. Joesten and S. L. Suib, *ChemCatChem*, 2013, **5**, 2306.
60 R. N. DeGuzman, Y. Shen, E. J. Neth, S. L. Suib, C. O'Young, S. Levine and J. M. Newsam, *Chem. Mater.*, 1994, **6**, 815.
61 L. Gong, Z. Huang, L. Luo and N. Zhang, *React. Kinet., Mech. Catal.*, 2014, **111**, 489.
62 X.-S. Liu, Z.-N. Jin, J.-Q. Lu, X.-X. Wang and M.-F. Luo, *Chem. Eng. J.*, 2010, **162**, 151.
63 W. Y. Hernández, M. A. Centeno, F. Romero-Sarria, S. Ivanova, M. Montes and J. A. Odriozola, *Catal. Today*, 2010, **157**, 160.
64 X. Ouyang and R. Besser, *J. Power Sources*, 2005, **141**, 39.
65 J. Giménez-Mañogil, A. Bueno-López and A. García-García, *Appl. Catal., B*, 2014, **152-153**, 99.
66 S. Veprek, D. L. Cocke, S. Kehl and H. R. Oswald, *J. Catal.*, 1986, **100**, 250.
67 H. Chen, X. Tong and Y. Li, *Appl. Catal., A*, 2009, **370**, 59.
68 M. Krämer, T. Schmidt, K. Stöwe and W. F. Maier, *Appl. Catal., A*, 2006, **302**, 257.
69 C. D. Wagner, W. M. Riggs, L. E. Davis, J. F. Moulder and G. E. Mullenberg, *Handbook of X-Ray Photoelectron Spectroscopy*, Perkin-Elmer Corporation, U.S.A., 1979.
70 A. Martínez-Arias, M. Fernández-García, J. Soria and J. C. Conesa, *J. Catal.*, 1999, **182**, 367.
71 G. Moretti, *J. Electron Spectrosc. Relat. Phenom.*, 1998, **95**, 95.
72 J. P. Espinós, J. Morales, A. Barranco, A. Caballero, J. P. Holgado and A. R. González-Elipe, *Appl. Catal., B*, 2002, **106**, 6921.
73 R. Hu, C. Yan, L. Xie, Y. Cheng and D. Wang, *Int. J. Hydrogen Energy*, 2011, **36**, 64.
74 F. Kapteijn, L. Singoredjo, A. Andreini and J. A. Moulijn, *Appl. Catal., B*, 1994, **3**, 173.
75 M. Piumetti, D. Fino and N. Russo, *Appl. Catal., B*, 2015, **163**, 277.
76 Y. Yang, J. Huang, S. Zhang, S. Wang, S. Deng, B. Wang and G. Yu, *Appl. Catal., B*, 2014, **150-151**, 167.
77 W. Y. Hernández, M. A. Centeno, S. Ivanova, P. Eloy, E. M. Gaigneaux and J. A. Odriozola, *Appl. Catal., B*, 2012, **123-124**, 27.
78 V. P. Santos, M. F. R. Pereira, J. J. M. Órfão and J. L. Figueiredo, *Appl. Catal., B*, 2010, **99**, 353.
79 L. M. Martínez, T. F. Romero-Sarria, W. Y. Hernández, M. A. Centeno and J. A. Odriozola, *Appl. Catal., A*, 2012, **423-424**, 137.
80 M. Özacar, A. S. Poyraz, H. C. Genuino, C.-H. Kuo, Y. Meng and S. L. Suib, *Appl. Catal., A*, 2013, **462-463**, 64.
81 W. Gac, *Appl. Catal., B*, 2007, **75**, 107.
82 F. C. Buciuman, F. Patcas and T. Hahn, *Chem. Eng. Process.*, 1999, **38**, 563.
83 J. Ashok, P. S. Reddy, G. Raju, M. Subrahmanyam and A. Venugopal, *Energy Fuels*, 2009, **23**, 5.
84 E. C. Njagi, C.-H. Chen, H. C. Genuino, H. Galindo, H. Huang and S. L. Suib, *Appl. Catal., B*, 2010, **99**, 103.
85 A. A. Mirzaei, H. R. Shaterian and M. Kaykhaii, *Appl. Surf. Sci.*, 2005, **239**, 246.
86 M. Navlani-García, B. Puértolas, D. Lozano-Castelló, D. Cazorla-Amorós, M. V. Navarro and T. García, *Environ. Sci. Technol.*, 2013, **47**, 5851.
87 S. Lowell, J. E. Shields, M. A. Thomas and M. Thommes, *Characterization of Porous Solids and Powders: Surface Area, Pore Size and Density*, Springer, 4th Revised Edition, 2006.
88 C. Almquist, M. Krekeler and L. Jiang, *Chem. Eng. J.*, 2014, **252**, 249.

